Thermo-optic Effects of Bragg Grating Optical Temperature Sensor

Kook-Chan Ahn*
Department of Mechanical Design Engineering
Jinju National University, Jinju, Korea 660-758

Sang-Mae Lee**
Center for Microelectronic Sensors and MEMS
Department of Electrical & Computer Engineering and Computer Science
University of Cincinnati, USA

Gwang-Seok Lee***
Department of Electronic Engineering
Jinju National University, Jinju, Korea 660-758

Seung-Bum Park****
Research Institute of Mechanical Technology
Pusan National University, Pusan, Korea 609-735

Abstract

This paper demonstrates a comparison of linear and nonlinear analyses for thermo-optic effects of optical temperature sensor based on the etched silica-based planar waveguide Bragg grating. Topics include theoretical analyses and experiment of the etched planar waveguide Bragg grating optical temperature sensor. Theoretical models with nonlinear than linear temperature effect for the grating response based on waveguide and plate deformation theories agree with experiments to within acceptable tolerance.

Key word : linear and nonlinear analyses, thermo-optic effects, optical temperature sensor

Introduction

High temperature strain measurements are critical to understanding constitutive properties of new high-temperature materials such as metal matrix composites (MMCs), ceramic matrix composites (CMCs) and carbon/carbon composites (CCCs) in wide applications involving advanced aeropropulsion systems or high speed civil transport. Strain gages most commonly used in high temperature measurements are based on resistance-based foil strain gages or capacitance-based strain gages, and are all limited to less than ~850℃. The recent entry in high temperature strain sensing field are transducers based on cylindrical optical waveguides produced from amorphous silica and sapphire. Silica based optical fiber sensors have been demonstrated up to 1,200℃, while sapphire-based sensors have been demonstrated in the

* Professor
E-mail : kcahn@jinju.ac.kr, TEL : 055-751-3352, FAX : 055-751-3359
** Researcher
*** Associate Professor
**** Researcher

temperature regime near 1,700℃. While sapphire sensors are attractive for high temperature sensor applications, they face a number of technical challenges. Optical grade sapphire fibers are difficult and expensive to fabricate, and only available in short segments. Additionally, the sapphire fiber sensors utilized the fiber Fabry-Perot interferometer thus far developed show limited promise for multiplexing. The silica-based sensors described in [1] and [2] face similar limitations with regard to multiplexing.

In-fiber Bragg grating sensors, on the other hand, have excellent multiplexing potential and therefore it is worth investigating how Bragg grating structures can be used to develop high temperature strain sensors.

This paper describes a comparison of linear and nonlinear analyses of optical temperature sensor based on the etched silica-based planar waveguide Bragg grating. Main topics include theoretical analyses and experiment of the etched planar waveguide Bragg grating optical temperature sensor. The functional operation of these sensors is then tested in uniform temperature fields with temperature up to 200℃. While this temperature range is modest in comparison with the stated target of 1,200℃, it lays the foundation for future development.

Theoretical Analyses

Mathematical Foundation

This basic mathematical foundation is used to analyze data of the proposed planar waveguide etched grating sensor. The waveguide geometry of interest is illustrated in Fig. 1 and consists of a germanium doped SiO_2 core bounded by air above and pure SiO_2 below. This waveguide is fabricated on a silicon substrate. The refractive indices of the air and the core and cladding SiO_2 layers are denoted by n_1, n_2, and n_3, respectively and core thickness is given by t_g. Also shown in Fig. 1 are the etched corrugations of pitch L and depth a.

The most important parameter in the design of Bragg grating in slab waveguides is effective index. This effective index is found by solving the wave equation and applying continuity boundary conditions at the respective core/cladding interfaces of the waveguide shown in Fig. 1. The guided modes have propagation constant β_s such that $k_0 n_3 < \beta_s < k_0 n_2$, where $n_1 < n_3$. This solution process leads to the following transcendental equation that yields the propagation constant:

$$\tanh t_g = \frac{p+q}{h(1-pq/h^2)} \tag{1}$$

where

$$h = (n_y^2 k_0^2 - \beta_s^2)^{1/2},\ q = (\beta_s^2 - n_1^2 k_0^2)^{1/2},\ p = (\beta_s^2 - n_3^2 k_0^2)^{1/2} \quad \text{and} \quad k_0 \cong \varpi / c = 2\pi / \lambda.$$

Given a set of the refractive indices n_1, n_2, and n_3 and the waveguide thickness, t_g of the planar waveguide, and the source wavelength, λ. Eq. (1) in general yields a number of solutions for the propagation constant β_s. However, the source wavelength and the waveguide thickness are restricted in the present study such that only one propagation mode is supported and therefore Eq. (1) has only one solution of interest. As a result, the effective index of the planar waveguide is given by $n_{eff} = \beta_s \lambda / 2\pi$. The corrugated structure into the waveguide leads to a corresponding periodic perturbation of the refractive index distribution. Each groove of the grating acts like a weak mirror and the cumulative effect of all of the weak reflectors results in a very strong combined reflection centered on what is known as the Bragg wavelength. The Bragg wavelength is related to the effective index calculated above and grating period L by [3]

$$\lambda_b = 2 n_{eff} \Lambda \tag{2}$$

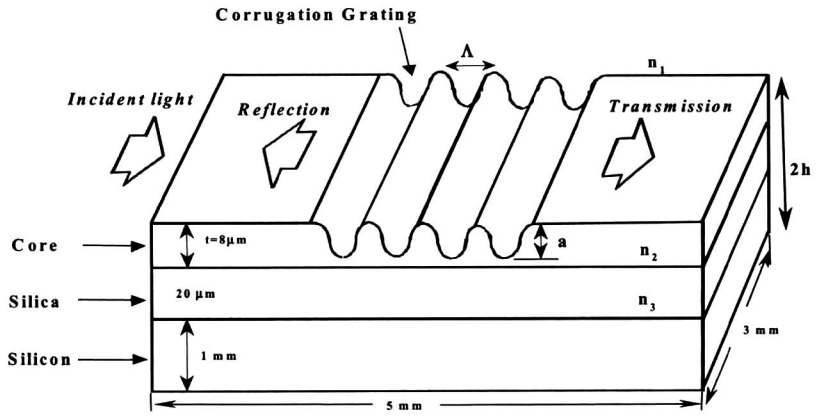

Fig. 1. Diagram of the slab waveguide with surface corrugation grating

which when expressed in terms of the propagation constant is given by

$$\lambda_b = \beta_s \lambda \Lambda / 2 \tag{3}$$

where λ_b is the Bragg wavelength and λ is the central wavelength of the optical source. The fraction of power coupled to the backward-propagation mode ($-\beta_s$), i.e. the grating reflectivity is given by [3]

$$\Re_{max} = \tanh^2(\kappa L) \tag{4}$$

where L is the length of the Bragg grating and the coupling coefficient k is given by [3]

$$\kappa = -\frac{2\pi^2}{3l\lambda}\frac{\left(n_2^2 - n_1^2\right)}{n_2}\left(\frac{a}{t_g}\right)^3\left[1 + \frac{3}{2\pi}\frac{\lambda/a}{\left(n_2^2 - n_1^2\right)^{1/2}} + \frac{3}{4\pi^2}\frac{\left(\lambda/a\right)^2}{\left(n_2^2 - n_1^2\right)}\right] \tag{5}$$

where l is the integer number of Bragg diffraction orders. Eqs. (1) through (5) are used to perform preliminary design of the planar waveguide grating sensor, and to guide the experimental program.

A change in the temperature of the planar waveguide causes a shift in the Bragg wavelength due to thermal expansion, and the thermo-optic change in the effective index. The temperature-induced fractional wavelength shift is given by [4]

$$\frac{\Delta\lambda_b}{\lambda_b} = (1 - p_e)\varepsilon_g + \xi\,\Delta T \tag{6}$$

where ε_g is the thermal strain in the guiding layer of the waveguide, P_e = 0.21 is the strain-optic coefficient for silica and ξ is the thermo-optic coefficient of the germanium-doped silica core.

The slab waveguide is composed of two layers of materials with different Youngs modulii and coefficients of thermal expansion. As a result, a change in temperature can cause a combination of expression of expansion and warping. The degree of warpage will depend on the mismatch in thermomechanical properties and difference in thicknesses. This type of mechanical system can be analyzed using Classical Laminated Plate Theory (CLPT) often utilized in the analysis of laminated composites structures. The incarnation of the CLPT used here is based on the following basic assumptions : (1) the layers within a laminate are considered perfectly bonded. (2) each layer is homogeneous. (3) each layer experiences plane stress conditions only. (4) plane sections remain plane. Following the CLPT approach, the strains on the surface of the waveguide is given by

$$\{\varepsilon\}=\{\bar{\varepsilon}^0\}+z\{\bar{k}\} \tag{7}$$

where $\{\bar{\varepsilon}^0\}$ is the global mid-plane strain, $\{\bar{k}\}$ is the global curvature and z is the distance from the laminate mid-plane to the plane on which the strain is to be calculated.

Linear Analysis

This analysis assumes that both the silica and silicon has isotropic mechanical properties. Table 1 provides the relevant properties [5].

Table 1. Materials properties of the silica and silicon

Materials	Thermal Expansion Coefficient, α(/℃)	Thermo-Optic Coefficient, ξ(/℃)	Young's Modulus, *E*(GPa)	Poisson's Ratio, ν
Silica	0.55	8.3	73	0.19
Silicon	2.63	--	190	0.27

The material properties in Table 1 are used with Eq. (7) to calculate the thermal strain in the core of the waveguide. This strain is the substituted into Eq. (6) to estimate the thermally induced change in the Bragg wavelength.

Nonlinear Analysis

The coefficient of thermal expansion for fused silica at temperatures between 0℃ to 50 0℃ can be given by [6]

$$\alpha_1(T) = a_1 + a_2T + a_3T^2 \tag{8}$$

where a_1 = 0.395 x 10^{-6}/℃, a_2 = 1.282 x 10^{-6}/℃, a_3 = -1.7 x 10^{-6}/℃. Similarly, the change in refractive index in the form of the differential variation for fused silica at given temperature between -200℃ to 640℃ is given by [7]

$$n_{eff}\xi = \frac{dn(T)}{dT} = b_1 + b_2T + b_3T^2 \tag{9}$$

where b_1 = 8.16638 x 10^{-6}, b_2 = 1.04124 x 10^{-8}, b_3 = -5.59781 x 10^{-12}. This functional form for the temperature dependence of the core and cladding refractive indices are used with Eqs. (1) through (3) to calculate the temperature dependent effective thermo-optic response of the waveguide.

As is given the coefficient of the fused silica above, the coefficient of thermal expansion for silicon at temperatures between -153℃ to 1,227℃ can be given [5]

$$\alpha_2(T) = 3.725 \text{ x } 10^{-6}[1-\exp(-5.88 \text{ x } 10^{-3}(T+149))]+5.548 \text{ x } 10^{-6}T \quad (\ /℃) \tag{10}$$

The CLPT can be provided details of how the mid-plane strains and curvatures are derived in terms of the Youngs modulii, coefficients of thermal expansion and thicknesses of SiO_2 waveguide and the silicon substrates. This analysis assumes that both the silica and silicon has isotropic mechanical properties. Table 2 provides the relevant properties [8]. Even though silicon is known to be anisotropic, the isotropy assumption is sufficient for the present analysis.

Table 2. Materials properties of the silica and silicon

Materials	Thermal Expansion Coefficient, α(/℃)	Thermo-Optic Coefficient, ξ(/℃)	Young's Modulus, *E*(GPa)	Poisson's Ratio, ν
Silica	Eq.(8)	Eq. (9)	73	0.19
Silicon	Eq.(10)	--	190	0.27

Experiment

The planar waveguides are fabricated by Photonics Integrated Research Inc.(PIRI) using hydrolysis deposition. These waveguides are originally manufactured with an 8mm thick germanium doped silica core with a 20mm silica undercladding sitting on top of a 1mm thick silicon substrate. The refractive indices of the core layer and undercladding layer are 1.4495 and 1.4452 measured at 1.55mm wavelength, respectively. The waveguide blank is diced parallel or perpendicular to the straight edge of the silicon substrate into 3mm long x 5mm wide waveguides.

The etched grating sensor is interrogated by using a single mode optical fiber to carry the light to and from the sensors. This means that efficient fiber to waveguide coupling techniques be used. Typical tolerance of lowest insertion loss are offset less than ±2mm and an angular misalignment less than 0.5℃. The butt coupling technique is shown schematically in [9, 10].

The exact center wavelength of the grating reflectivity will vary with the effective index of the guided mode, which itself depends on the waveguide dimensions. As part of the grating evaluation process, the effective indices of the slab waveguides were measured using the intermodal spacing in the optical spectra produced by a Fabry-Perot interferometer purposefully formed between the two facets of the waveguide. This effective index is given by

$$n_{eff} = \lambda_o^2 / (2\delta\lambda L_w) \tag{11}$$

where λ_0 is the peak emission wavelength, $\delta\lambda$ is intermodal spacing of the waveguide cavity and L_w is the length of the cavity. The intermodal spacing of the waveguide cavity is measured using the EDFA in the arrangement shown in [9, 10]. In this case, however, steps are taken to promote Fabry-Perot interference between the two waveguide facets. This involves keeping a 1μm gap between the optical fiber lead and front facet, and not using index matching liquid on the back facet. The resulting optical spectrum is viewed using an Advantest, Model Q8347 optical spectrum analyzer. This particular OSA enables the intermode spacing measurements 0.007nm wavelength resolution.

The reflected spectrum produced by a grating 2mm long, 200nm deep (typical values) etched into a planar waveguide was measured with the optical spectrum analyzer as well. The reflected spectrum of the reflection from the planar waveguide gratings generally appeared bifurcated due to geometry-induced birefringence. Therefore, an output fiber polarizer is used to isolate the Bragg condition from one polarization mode. In order to examine temperature sensing performance of the etched planar waveguide Bragg grating sensor, the planar waveguide Bragg grating was heated with temperature ranging from 20℃ to 200℃ using the heating tape which fold the translating block mounting the planar waveguide.

Results and Discussion

Fig. 2 shows the reflected spectrum produced by a grating 2mm long, 200nm deep (typical values) etched into a planar waveguide. The reflected spectrum of the reflection from the planar waveguide gratings generally appeared bifurcated due to geometry-induced birefringence. Therefore, an output fiber polarizer is used to isolate the Bragg condition from one polarization mode. However, the birefringent bifurcation of the waveguide in the present study was disappeared with high temperature during measuring the temperature. Typical values for the grating bandwidth and reflectivity are 0.2nm and ~0.7%, respectively. To compare the calculated with measured, the only one experimental point was able to be shown because the reflectivity can be predicted only at room temperature although the experimental results obtained at elevated temperature could be available. The reflectivity of this grating calculated with Eq. (4) and L = 2.0mm and a = 200nm is 7.1%, which agrees with the experiments to within 1.4% of the calculated value.

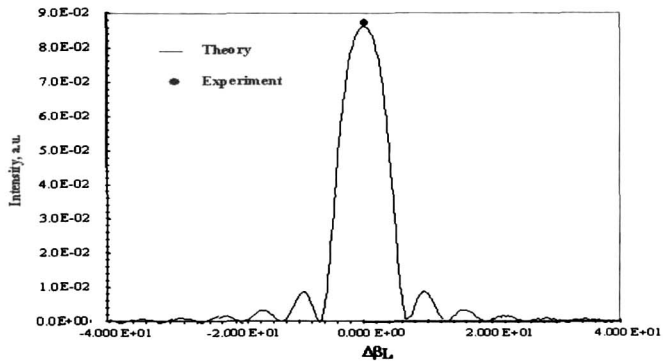

Fig. 2. Reflectivity of the etched planar waveguide Bragg grating sensor

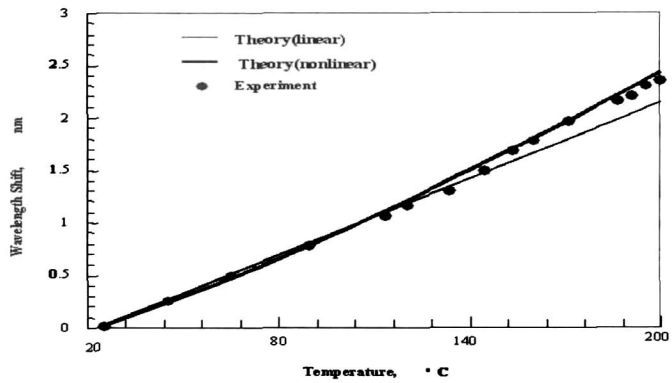

Fig. 3. Comparison of shifts in Bragg wavelength induced by temperature changes

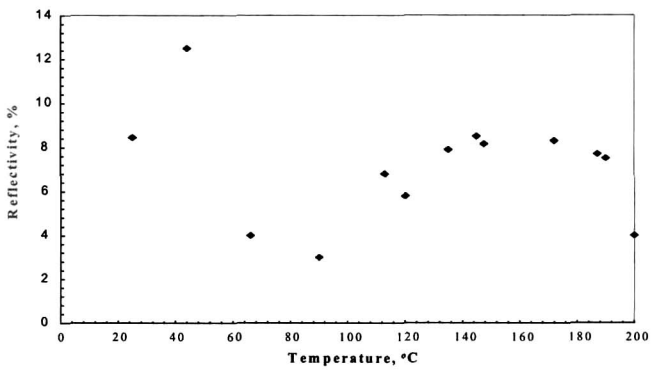

Fig. 4. Reflectivity of Bragg wavelength in etched planar waveguide grating sensor with temperature changes

Fig. 3 provides a graph of Bragg wavelength as a function of temperature measured using a spectrum analyzer. The material properties in Table 1 and 2 are used with Eq. (7) to calculate the thermal strains for linear and nonlinear analyses in the core of the waveguide. These strains are the substituted into Eq. (6) to estimate the thermally induced change in the Bragg wavelength.

For linear(nonlinear) analysis, this calculation leads to a proportionality factor of 0.0122nm/℃ (0.0137nm/℃) between the change in wavelength and temperature, as shown in Fig. 3. For comparison, the proportionality factor for a 1,550nm photorefractive grating written in an optical fiber is 0.0132nm/℃.

The thin(thick) solid line in this figure is the wavelength response calculated using linear(nonlinear) theory. For linear analysis, the temperature-induced fractional Bragg

wavelength shift measured in this experiment is 7.5% upper than the calculated value. However, it is hard to compare the measured with the theoretical because the measured results show slightly nonlinear slope.

For nonlinear analysis, the measured sensitivity is 3.6% lower than the calculated value, which agrees with experiments better than that of linear analysis as the temperature increases up to 200℃.

Fig. 4 shows the reflectivity at the Bragg wavelength as a function of temperature. As shown in this figure, the reflectivity increases at temperature, 44℃. Up to about 100℃, the reflectivity in decreased but the reflectivity remains stable from 100℃. The origins of this effect are not clear, but a silica overcladding would likely reduce the variability.

Conclusions

The analyses of optical temperature sensor based on the etched planar waveguide Bragg grating were explored using the theoretical and the experimental techniques. Classical laminated plate theories used with linear and nonlinear temperature effects were combined in a simple model for the grating temperature response to predict the response of the temperature sensor. Theoretical models with nonlinear than linear temperature effect agree with experiments to within acceptable tolerance as the temperature increases. Therefore these theoretical predictions showed that the non-linear behaviors of the sensor can be important at higher temperature. This paper has demonstrated only the first step in developing high temperature strain gages and temperature sensors.

Acknowledgement

This work was supported by the Korea Science and Engineering Foundation (KOSEF) through the Regional Animal Industry Research Center. (Project No. : R12-2002-053-02003-0)

References

1. Chang, C. C., Sagrario, D., Job, L. and Sirkis, J. S., Using Standard Interferometric Sensors for High Temperature Strain Measurements, SPIE Vol. 2191, pp. 482-486, 1994.

2. Lee, C. E. and Taylor, H. F., IEEE Journal of Lightwave Technology, 9, 129, 1991.

3. Yariv, A., Coupled-Mode Theory for Guided-Wave Optics, IEEE Journal of Quantum Electronics, Vol. 9, pp. 919-933, 1973.

4. Morey, W. W., Meltz, G. and Glenn, W. H., Fiber Optic Bragg Grating Sensors, Fiber Optic and Laser Sensors VII, SPIE Vol. 1169, pp. 98-107, 1989.

5. Petersen, K. E., Proceedings of IEEE, Vol. 70, 1982.

6. Malitson, I. H., Interspecimen Comparison of the Refractive Index of Fused Silica, J. Opt. Soc. America, Vol. 55, No. 10, pp. 1205-1210, 1965.

7. Waxler, M. and Cleek, G. W., The Effect of Temperature and Pressure on the Refractive Index of Some Sxide Glasses, J. Res. Nat. Bureau of Stan., Vol. 77A, No. 6, pp. 755-763, 1973.

8. Izawa, T., More, H., Murakami, Y. and Shimizu, N., Deposited Silica Waveguide for Integrated Optical Circuits, Applied Physics Letters, Vol. 38, No. 7, pp. 483-485, 1981.

9. Lee, S. M., Ahn, K. C. and Sirkis, J. S., Planar Optical Waveguide Temperature Sensor Based on Etched Bragg Gratings Considering Nonlinear Thermo-optic Effect, KSME International Journal, Vol. 15, No. 3, pp. 309-319, 2001.

10. Ahn, K. C. and Lee, S. M., The Development of Optical Temperature Sensor on the Etched Bragg Gratings, KSAS International Journal, Vol. 2, No. 2, pp. 56-64, 2001.